


# The Performance of the Athena X-ray Integral Field Unit at Very High Count Rates

Philippe Peille<sup>1</sup>  · T. Dauser<sup>2</sup> · C. Kirsch<sup>2</sup> ·  
R. den Hartog<sup>3</sup> · E. Cucchetti<sup>4</sup> · J. Wilms<sup>2</sup> ·  
D. Barret<sup>4</sup> · J.-W. den Herder<sup>3</sup> · L. Piro<sup>5</sup>

Received: 4 November 2017 / Accepted: 10 May 2018 / Published online: 30 May 2018  
© Springer Science+Business Media, LLC, part of Springer Nature 2018

**Abstract** The Athena X-ray Integral Field Unit (X-IFU) will operate at 90 mK a hexagonal matrix of 3840 Transition Edge Sensor pixels providing spatially resolved high-resolution spectroscopy (2.5 eV FWHM up to 7 keV) between 0.2 and 12 keV. During the observation of very bright X-ray sources, the X-IFU detectors will receive high photon rates going up to several tens of counts per second per pixel and hundreds per readout channel, well above the normal operating mode of the instrument. In this paper, we investigate through detailed end-to-end simulations the performance achieved by the X-IFU at the highest count rates. Special care is notably taken to model and characterize pulse processing limitations, readout-chain saturation effects, as well as the non-Gaussian degradation of the energy redistribution from crosstalk at the focal plane level (both thermal and electrical). Overall, we show that the instrument performance should safely exceed the scientific requirements, and in particular that more than 50 % throughput at 1 Crab in the 5–8 keV band can be achieved with better than 10 eV average resolution with the use of a Beryllium filter, enabling breakthrough science in the field of bright sources.

---

✉ Philippe Peille  
philippe.peille@cnes.fr

- <sup>1</sup> Centre National d'Etudes Spatiales, Centre Spatial de Toulouse, 18 Avenue Édouard Belin, 31400 Toulouse Cedex 9, France
- <sup>2</sup> ECAP, University of Erlangen-Nuremberg, Sternwartstr. 7, 96049 Bamberg, Germany
- <sup>3</sup> SRON, Netherlands Institute for Space Research, Sorbonnelaan 2, 3584 CA Utrecht, The Netherlands
- <sup>4</sup> IRAP, Université de Toulouse, CNRS, UPS, CNES, Toulouse, France
- <sup>5</sup> IAPS, Istituto di Astrofisica e Planetologia Spaziali, Via Fosso del Cavaliere 100, 00133 Rome, Italy

**Keywords** X-IFU · X-ray microcalorimeters · TES · Crosstalk · FDM

## 1 Introduction

Planned for launch onboard the Athena X-ray Observatory [1], the X-ray Integral Field Unit [2,3] is a high-resolution imaging spectrometer designed to observe the soft X-ray band using a matrix of  $\sim 4000$  Transition Edge Sensor (TESs) microcalorimeters operated in a setpoint temperature around 90 mK. Its readout scheme uses Frequency Domain Multiplexing (FDM) in the 1–5 MHz band, with a multiplexing factor of 40 [4,5] and an output sampling rate of 156.25 kHz. With its unprecedented energy resolution of 2.5 eV (FWHM at 7 keV) and a field of view of  $5^\circ$ , associated with the Athena optics (more than  $1.4 \text{ m}^2$  effective area), it will allow breakthrough science in a very large set of science fields. During most of its observations, the X-IFU pixels will receive count rates largely below 1 count/s (cps), but for certain very bright sources, such as supernova remnants or galactic black holes, the instrument will see photon rates going up to several tens of cps/pixel and hundreds per readout channel. In this regime, usually negligible degradations such as pile-up, crosstalk and readout-chain nonlinearities will start to play a role. Here, we investigate through detailed end-to-end simulations the X-IFU performance at these highest count rates.

## 2 Simulation Setup

This study was performed in the SIXTE framework (SIMulations of X-ray TELEscopes<sup>1</sup>, [6]). It is a modular software suite developed to allow end-to-end simulations of various X-ray missions, including the Athena observatory. In a Monte-Carlo process, photons are generated from a source catalog and then followed through the full imaging and detection process. Therein, the telescope, together with the X-IFU filters, is modeled through a set of calibration files allowing to properly distribute the photon impacts, with relevant energy and timing properties, onto the focal plane, in the various configurations foreseen. It notably allows to simulate mirror defocusing, which was recently introduced in the Athena concept to ease the observation of the brightest point sources: the mirror being integrated on a hexapod platform, it is possible to move it away from the focal plane by up to 35 mm, going from a narrow point spread function illuminating  $\sim 5$  pixels to a broad one over  $\gtrsim 600$  pixels (see, e.g., [2]). A detailed description of the X-IFU matrix hexagonal geometry is then used to associate these events to the impacted pixels and corresponding readout channels. At the end of the process, the readout energy of each event is computed through a set of response matrices and coupling mechanisms taking into account notably the degradation of the instrument performance with count rate. This last step was specifically modified in the frame of this study and will be described here in greater detail. It should be noted that the X-IFU Event Processor and the Athena spacecraft are being designed such that

<sup>1</sup> <http://www.sternwarte.uni-erlangen.de/research/sixte/>.

**Table 1** Definition of the different event grades in the simulation, with a sampling rate of 156.25 kHz

Grade	Time since previous pulse	Time until next pulse	Filter length	Energy resolution
High res.	$\geq 7.9$ ms	$\geq 45.3$ ms	7080 samples	2.5 eV
Medium res.	$\geq 7.9$ ms	$\geq 2.3$ ms	354 samples	3 eV
Limited res.	$\geq 7.9$ ms	$\geq 1$ ms	146 samples	7 eV
Low res.	$\geq 7.9$ ms	–	4 samples	$\sim 30$ eV

onboard processing power and telemetry rates will not be a limiting factor for high count rates observations. These limitations can therefore be ignored here.

## 2.1 Event Reconstruction Limitations

The X-IFU pixels will be operated as microcalorimeters: when a photon impacts, it will thermalize in an absorber strongly thermally linked to the TES whose temperature will increase, leading to a rapid change in resistance and thus a current pulse. This signal will be used onboard to estimate the energy of the event, typically through the application of an optimal filter [7]. At high count rates, the current pulses will get packed together in the pixels' timelines, leading to two main degradations of the instrument performance. For each event, if the preceding pulse is too close, the energy reconstruction will be biased and the event will need to be rejected from the high-resolution data. Such events are called secondaries. A nearby subsequent pulse will in turn prevent the use of the longest optimal filter to perform the reconstruction and degrade the energy resolution. To characterize these effects, different grades were defined in the simulator depending on the time separation of the pulses in a similar way to, e.g., [8]. These were computed using the main speed characteristics of the future X-IFU pixels ("hybrid LPA" in [9]) and are summarized in Table 1.

Here, we took a conservative approach and assumed secondaries correspond to a rejection interval of 10 times the pixel electro-thermal feedback time constant ( $\sim$  pulse fall time in the low inductance limit), whereas the pixels will actually be operated under critical damping conditions [9]. For the remaining valid events, the relation between the available record length and the achieved energy resolution is given by  $\Delta E(t_{\text{rec}}) = \frac{\lim_{t_{\text{rec}} \rightarrow \infty} \Delta E}{\sqrt{1-1/(2t_{\text{rec}} f_{\text{eff}})}}$  [10]. At the detection step, the software thus computes the grade of each event and uses a response matrix of the corresponding energy resolution to randomize the readout energy accordingly.

## 2.2 Crosstalk

At the highest count rates, the fraction of overlapping events increases and the effect of crosstalk can become dominant. We define crosstalk as any science signal, originating from the absorption of energy on one (perpetrator) pixel, contributing to an energy measurement on another (victim) pixel. At present, we simulate three main general

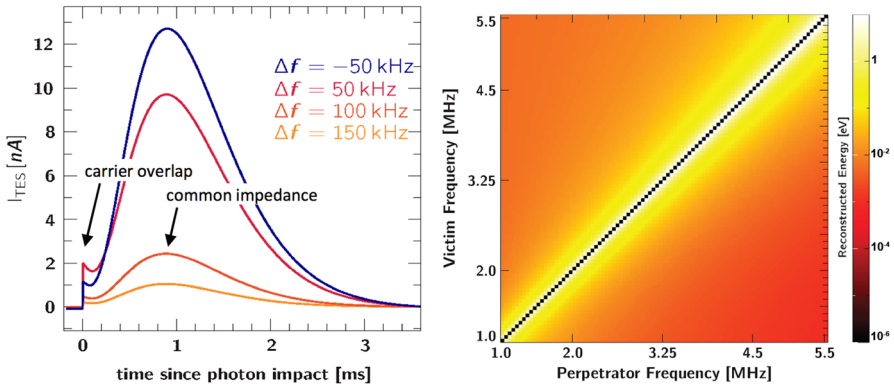


**Fig. 1** *Left:* Crosstalk pulses with the carrier overlap and common impedance components. *Right:* Slice of the electrical crosstalk lookup table (perpetrator energy equal to 13.8 keV) showing the characterization of the frequency dependence of the crosstalk for high-resolution events (Color figure online)

sources of crosstalk: electrical crosstalk due to the FDM process, thermal crosstalk at the level of the TES array, and nonlinearity crosstalk originating from the nonlinearity of the readout.

### 2.2.1 Electrical Crosstalk

Due to the FDM readout of the X-IFU pixels, part of the signal generated by an event in one pixel will appear in the readout of the other pixels sharing the same readout channel. In order to characterize this effect, detailed simulations of the first-stage readout circuit were conducted with a specific tool in the SIXTE software (*tessim*, [11]). Two main crosstalk types were identified: a fast component due to the finite quality factor of the LC filters (carrier overlap) and a slower thermal response of the victim pixel to the current change in the perpetrator pixel through the common impedance in the circuit—mainly the SQUID input coil (see Fig. 1, left, for example crosstalk signals). More details on this crosstalk modeling and its first experimental verification can be found in [12].

To characterize the energy and frequency dependence of the electrical crosstalk in the simulator, crosstalk-affected pulses were computed for a set of frequency couples and perpetrator energies in the case when the events in the two pixels arrived at the same time. The resulting signal was then reconstructed with an optimal filter in order to obtain an effective energy influence of the crosstalk onto the victim pulse that was saved in lookup tables (see Fig. 1, right). Because of the shape of the filters used for the reconstruction (see, e.g., [13]), this influence will actually depend on the phasing of the events. This was characterized for the different filter lengths using 1 keV victim events as shown in Fig. 3 (left).

### 2.2.2 Thermal Crosstalk

Thermal crosstalk is the result of thermal coupling between physically adjacent pixels, where thermal power flows from a pixel which has been heated by an incident photon

(perpetrator) to other victim pixels or the array. In [14, 15], this crosstalk has been measured at the level of  $10^{-3}$  for first neighbor pixels for 8x8-pixel arrays. The magnitude and actual shape of this effect strongly depends on the layout and construction of the actual array. For simplicity reasons, thermal crosstalk was therefore modeled as a simple scaled energy transfer from the perpetrator event onto the neighboring pixel. The actual influence on the energy reconstruction of the victim pulses was then computed using the same time dependency weighting as for the electrical crosstalk (see Fig. 3, left). In this study, we took the levels of crosstalk measured in [15] in the presence of a backside copper layer, as foreseen for the X-IFU (could be gold, [16]), i.e.,  $10^{-3}$  for the first neighbor,  $4 \times 10^{-4}$  for diagonal neighbors, and  $8 \times 10^{-5}$  for second neighbors.<sup>2</sup>

### 2.2.3 Nonlinearity Crosstalk

Although nonlinearity crosstalk can originate in every element of the amplifier chain, only the first-stage SQUID is considered here, as its nonlinearity is expected to be dominant. The SQUID transfer function is (approximately) sinusoidal and will therefore naturally create higher-order harmonic terms when the signals from two pixels arrive at the same time at its input. This will result in a modification of the demodulated signal of both events and therefore a shift in their reconstructed energies. In practice, this effect will be limited by the use of a baseband feedback loop (BBFB, [4, 17]) which will reduce the excursion of the error signal. To characterize this effect, we therefore conducted detailed BBFB simulations of sets of two incident pulses and reconstructed their energy using standard optimal filtering. The measured energy shifts were then saved in lookup tables as a function of the events energies, and their time and frequency separation, in a similar way to what was done for the electrical crosstalk.

## 3 X-IFU Performance at Very High Count Rates

Using the setup described above, we performed full end-to-end simulations of the three most challenging science cases of the X-IFU observing plan in terms of count rate capability:

- On-focus high-resolution observation of a bright extended source. This typically corresponds to the study of a supernova remnant, like Cas A, or the center of a cluster like Perseus. We took an absorbed thermal emission at 5 keV over a flat field to model this. The average energy of the impacts is 1.7 keV.
- Defocussed (35 mm) high-resolution observation of a bright point source. This would be associated with the observation of bright gamma ray burst afterglows. This was simulated with the same spectral distribution as the Crab pulsar and nebula, i.e., an absorbed power-law of photon index 2.1. At 10 mCrab,  $\gtrsim 600$

---

<sup>2</sup> We note that with their lower bath conductivity compared to the pixels presented in these papers, the X-IFU pixels should in principle see smaller levels of thermal leakage than measured in these previous devices.

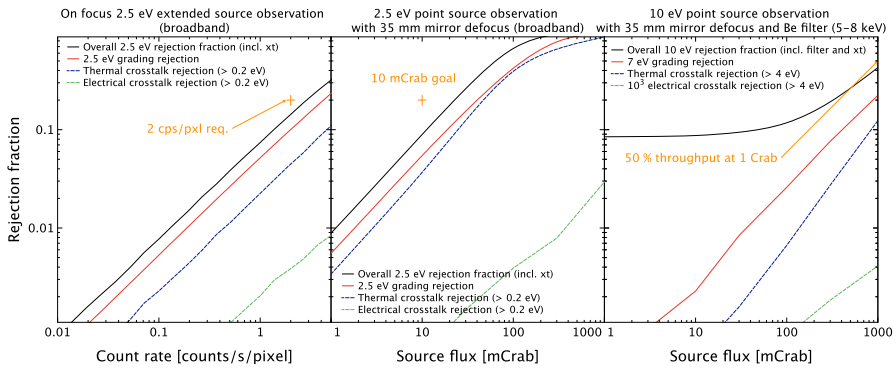


**Fig. 2** Fraction of events rejected for different types of observations as a function of count rate or source flux. *Left:* High-resolution observation of an extended source with a thermal spectrum observed on focus. *Middle:* High-resolution observation of a bright defocused (35 mm) point source with a Crab-like spectrum. 10 mCrab corresponds to 900 cps over the array. *Right:* 10 eV resolution observation of the same source but with the use of a 100  $\mu\text{m}$  Be filter. 1000 mCrab thus corresponds to 17,000 cps over the array. The X-IFU performance requirements are indicated in orange. Nonlinearity crosstalk is negligible in all cases (Color figure online)

pixels have count rates higher than 0.8 cps, with a maximum of 1.6 cps and an average photon energy of 1.5 keV, for a total of 900 cps over the array.

- Defocused (35 mm) observation of a very bright Crab-like point source, with degraded resolution and the use of a 100  $\mu\text{m}$  thick beryllium filter suppressing most of the  $< 3$  keV events. At 1 Crab, the total count rate is thus reduced to 17,000 cps, with the brightest pixels receiving  $\sim 40$  cps and  $\sim 200$  pixels receiving more than 20 cps, with an average energy of 3.35 keV. This science case corresponds to the study of black hole winds that generate blue-shifted iron lines, to be studied in the 5–8 keV range.

As described above, in these simulations, we model crosstalk as additional energy offsets affecting the events depending on the presence of neighboring impacts (either spatially or in readout frequency). This will effectively modify the instrument energy redistribution function. As a first simplified approach, events affected by crosstalk above a certain energy offset limit are accounted as throughput loss: for high-resolution events, this limit is put at 0.2 eV (corresponds to the allocation in the X-IFU energy resolution budget), whereas for limited resolution events, we used 4 eV to ensure a better than 10 eV final resolution (which corresponds to the scientific need to separate the H-like Fe XXVI doublet) starting from the 7-eV crosstalk-free performance (see Table 1). We note that this assumes an a priori knowledge of the crosstalk effect, which is deterministic, so that affected events can be rejected, but no post-correction to repair the crosstalk influence is applied.

Figure 2 shows the results of the simulations with the contribution of the different rejection mechanisms. In all cases, the predicted performance of the instrument safely exceeds the requirements, which shows again how the X-IFU capabilities were improved thanks to mirror defocusing [2]. For extended sources, count rates up to 3 cps/pixel can be achieved, whereas defocused point sources two times brighter than

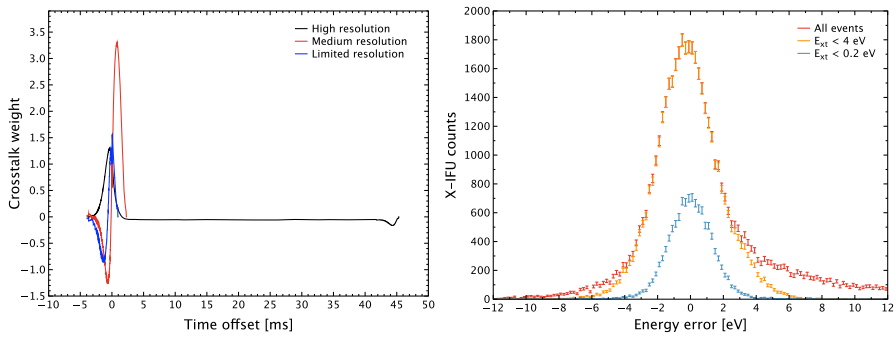


**Fig. 3** *Left:* Dependence of the electrical crosstalk level on the difference in arrival time between photons on the victim and perpetrator pixels for different filter lengths. *Right:* Energy redistribution measured between 6 and 7 keV in a 50 s simulation of a 1 Crab source with 35 mm defocusing and a Be filter (Color figure online)

the requirement can be observed with 80% throughput of high-resolution events. For the brightest observations, the inclusion of a Beryllium filter allows to reach fluxes up to 1 Crab with more than 50% throughput at high energy of 10 eV events.<sup>3</sup> Overall, the count rate capability of the instrument is found to be mainly limited by event grading, closely followed by thermal crosstalk, notably for the point sources as the events are less evenly spread over the detection matrix despite defocussing. This confirms that special care should be taken in the heatsinking of the TES array. The electrical crosstalk appears to be at least an order of magnitude weaker, showing that there is some margin for an underprediction of the model.

In the end-to-end simulator, as we follow each photon from its original emission by the source to the final recorded energy, we can have a closer look at the realized energy redistribution including the effect of crosstalk. In Fig. 3 (right), we show the one that was measured between 6 and 7 keV in a 1 Crab simulation. If no cut is performed on crosstalk influence, significant non-Gaussianities are present, as well as a small average energy offset. If we now reject the most affected events ( $> 4$  eV), the main effect of crosstalk is a symmetrical broadening leading to an energy resolution around 6 eV FWHM, showing a further margin on the X-IFU count rate capability at 1 Crab. This is due to the effect of the optimal filtering that generates from mostly positive crosstalk signals (thermal crosstalk is dominating) in turns positive and negative offsets (see Fig. 3, left).

## 4 Conclusion

In this paper, we have presented detailed end-to-end simulations of the X-IFU performance at the highest fluxes it will observe. In this regime, special care had to be taken

<sup>3</sup> We note that most bright sources actually have a thicker absorption column density than the Crab, which was used here. This creates already a significant low energy cutoff, even without filter. Provided their flux in the 3–12-keV band is lower than the Crab, they could therefore be observed with a thinner filter. For this reason, a second, thinner filter, is considered as a goal for the X-IFU filter wheel.

to model the effect of energy reconstruction limitations, but also of various crosstalk mechanisms. Overall, we showed that the instrument should safely exceed its performance requirements. Of course, the assumptions taken here warrant experimental verification, notably the electrical crosstalk model which has only started to be verified [12]. Further improvements in the instrument performance will also be investigated in the future like a partial event-based post-correction of the crosstalk influence instead of the rejection assumed here, or the use of resistance space optimal filtering which has been shown to perform better for short record lengths [18].

**Acknowledgements** This work has been partially funded by the Bundesministerium für Wirtschaft und Technologie under Deutsches Zentrum für Luft- und Raumfahrt Grant 50 QR 1402.

## References

1. K. Nandra, D. Barret, X. Barcons, A. Fabian, J.-W. den Herder, L. Piro, M. Watson, C. Adami, J. Aird, J.M. Afonso et al., The hot and energetic universe: a white paper presenting the science theme motivating the Athena+ mission (2013). <https://ui.adsabs.harvard.edu/#abs/2013arXiv1306.2307N>
2. D. Barret, T. Lam Trong, J.-W. den Herder, L. Piro, X. Barcons, J. Huovelin, R. Kelley, J.M. Mas-Hesse, K. Mitsuda, S. Paltani, G. Rauw, A. Rozanska, J. Wilms, M. Barbera, E. Bozzo, M.T. Ceballos, I. Charles, A. Decourchelle, R. den Hartog, J.-M. Duval, F. Fiore, F. Gatti, A. Goldwurm, B. Jackson, P. Jonker, C. Kilbourne, C. Macculi, M. Mendez, S. Molendi, P. Orleanski, F. Pajot, E. Pointecouteau, F. Porter, G.W. Pratt, D. Prêle, L. Ravera, E. Renotte, J. Schaye, K. Shinozaki, L. Valenziano, J. Vink, N. Webb, N.Y. Yamasaki, The Athena X-ray integral field unit (X-IFU). *Proc. SPIE* **9905**, 9905–83 (2016)
3. F. Pajot, D. Barret, T. Lam Trong, J.-W. den Herder, L. Piro and M. Cappi. and M. Cappi., The Athena x-ray integral field unit *J. Low Temp. Phys.*, This Special Issue LTD17 (2018). <https://doi.org/10.1007/s10909-018-1904-5>
4. H. Akamatsu, L. Gottardi, J. van der Kuur, C.P. de Vries, K. Ravensberg, J.S. Adams, S.R. Bandler, M.P. Bruijn, J.A. Chervenak, C.A. Kilbourne, M. Kiviranta, A.J. van der Linden, B.D. Jackson, S.J. Smith, Development of frequency domain multiplexing for the X-ray integral field unit (X-IFU) on the Athena. *Proc. SPIE* **9905**, 99055S (2016). <https://doi.org/10.1117/12.2232805>
5. H. Akamatsu, L. Gottardi, J. van der Kuur, C.P. de Vries, M.P. Bruijn, J.A. Chervenak, M. Kirivanta, A.J. van den Linden, B.D. Jackson, S.J. Smith, Frequency domain multiplexed readout of tes X-ray microcalorimeters for X-ifu on board of Athena *J. Low Temp. Phys.*, This Special Issue LTD17 (2018)
6. J. Wilms, T. Brand, D. Barret, T. Beuchert, J.-W. den Herder, I. Kreykenbohm, S. Lotti, N. Meidinger, K. Nandra, P. Peille, L. Piro, A. Rau, C. Schmid, R.K. Smith, C. Tenzer, M. Wille, R. Willingale, ATHENA end-to-end simulations. *Proc. SPIE* **9144**, 91445X (2014). <https://doi.org/10.1117/12.2056347>
7. A.E. Szymkowiak, R.L. Kelley, S.H. Moseley, C.K. Stahle, Signal processing for microcalorimeters. *J. Low Temp. Phys.* **93**(3), 281–285 (1993). <https://doi.org/10.1007/BF00693433>. ISSN 1573-7357
8. H. Seta, M.S. Tashiro, Y. Ishisaki, M. Tsujimoto, Y. Shimoda, Y. Abe, T. Yasuda, S. Takeda, M. Asahina, Y. Hiyama, S. Yamaguchi, Y. Terada, K.R. Boyce, F.S. Porter, C.A. Kilbourne, R.L. Kelley, R. Fujimoto, Y. Takei, K. Mitsuda, K. Matsuda, K. Masukawa, The digital processing system for the soft X-ray spectrometer onboard ASTRO-H—the design and the performance. *IEEE Trans. Nucl. Sci.* **59**, 366–372 (2012). <https://doi.org/10.1109/TNS.2011.2179671>
9. S.J. Smith, J.S. Adams, S.R. Bandler, J.L. Betancourt-Martinez, J.A. Chervenak, M. Chiao, A.M. Datesman, M.E. Eckart, A.J. Ewin, F.M. Finkbeiner, R.L. Kelley, C.A. Kilbourne, F.S. Porter, J.E. Sadleir, E.J. Wassel, W. Yoon, D.A. Bennett, W.B. Doriese, G.C. Hilton, D.S. Swetz, J.N. Ullom, H. Akamatsu, L. Gottardi, R.H. den Hartog, B.D. Jackson, J. van der Kuur, D. Barret, P. Peille, TES pixel parameter design of the microcalorimeter array for the X-ray integral field unit on ATHENA. *Proc. SPIE* **9905**, 9905–85 (2016)
10. W.B. Doriese, J.S. Adams, G.C. Hilton, K.D. Irwin, C.A. Kilbourne, F.J. Schima, J.N. Ullom, Optimal filtering, record length, and count rate in transition-edge-sensor microcalorimeters. *Am. Inst. Phys. Conf. Ser.* **1185**, 450–453 (2009). <https://doi.org/10.1063/1.3292375>



11. J. Wilms, S.J. Smith, P. Peille, M.T. Ceballos, B. Cobo, T. Dausser, T. Brand, R. den Hartog, S.R. Bandler, J. de Plaa, J.-W. den Herder, TESSIM: a simulator for the ATHENA X-IFU. *Proc. SPIE* **9905**, 91445Q (2016). <https://doi.org/10.1117/12.2056434>
12. R. den Hartog, C. Kirsch, C. de Vries, H. Akamatsu, T. Dausser, P. Peille, E. Cucchetti, S.R. Bandler, S.J. Smith, J. Wilms, Crosstalk in an fdm laboratory set-up and the athena X-ifu science performance. *J. Low Temp. Phys.*, This Special Issue LTD17 (2018). <https://doi.org/10.1007/s10909-018-1912-5>
13. K.R. Boyce, M.D. Audley, R.G. Baker, J.J. Dumonthier, R. Fujimoto, K.C. Gendreau, Y. Ishisaki, R.L. Kelley, C.K. Stahle, A.E. Szymkowiak, G.E. Winkert, Design and performance of the ASTRO-E/XRS signal processing system. *Proc. SPIE* **3765**, 741–750 (1999)
14. C.A. Kilbourne, W.B. Doriese, S.R. Bandler, R.P. Brekosky, A.-D. Brown, J.A. Chervenak, M.E. Eckart, F.M. Finkbeiner, G.C. Hilton, K.D. Irwin, N. Iyomoto, R.L. Kelley, F.S. Porter, C.D. Reintsema, S.J. Smith, J.N. Ullom, Multiplexed readout of uniform arrays of TES X-ray microcalorimeters suitable for Constellation-X. *Proc. SPIE* **7011**, 701104 (2008). <https://doi.org/10.1117/12.790027>
15. N. Iyomoto, S.R. Bandler, R.P. Brekosky, A.-D. Brown, J.A. Chervenak, E. Figueroa-Feliciano, F.M. Finkbeiner, R.L. Kelley, C.A. Kilbourne, F.S. Porter, J.E. Sadleir, S.J. Smith, Heat sinking and crosstalk for large, close-packed arrays of microcalorimeters. *J. Low Temp. Phys.* **151**, 506–512 (2008). <https://doi.org/10.1007/s10909-007-9682-5>
16. S.J. Smith, J.S. Adams, S.R. Bandler, S.E. Busch, J.A. Chervenak, M.E. Eckart, F.M. Finkbeiner, R.L. Kelley, C.A. Kilbourne, S.J. Lee, J.-P. Porst, F.S. Porter, J.E. Sadleir, Characterization of Mo/Au transition-edge sensors with different geometric configurations. *J. Low Temp. Phys.* **176**, 356–362 (2014). <https://doi.org/10.1007/s10909-013-1031-2>
17. L. Ravera, C. Cara, M.T. Ceballos, X. Barcons, D. Barret, R. Clédassou, A. Clénet, B. Cobo, E. Doumayrou, R.H. den Hartog, B.-J. van Leeuwen, D. van Loon, J.M. Mas-Hesse, C. Pigot, E. Pointecouteau, The DRE: the digital readout electronics for ATHENA X-IFU. *Proc. SPIE* **9144**, 91445T (2014). <https://doi.org/10.1117/12.2055750>
18. P. Peille, M.T. Ceballos, B. Cobo, J. Wilms, S. Bandler, S.J. Smith, T. Dausser, T. Brand, R. den Hartog, J. de Plaa, D. Barret, J.-W. den Herder, L. Piro, X. Barcons, E. Pointecouteau, Performance assessment of different pulse reconstruction algorithms for the ATHENA X-ray integral field unit. *Proc. SPIE* **9905**, 99055W (2016). <https://doi.org/10.1117/12.2232011>